

## GLOBULAR AND OPEN CLUSTERS OBSERVED BY SDSS/SEGUE: THE GIANT STARS

HEATHER L. MORRISON<sup>1</sup>, ZHIBO MA<sup>1</sup>, JAMES L. CLEM<sup>2</sup>, DEOKKEUN AN<sup>3</sup>, THOMAS CONNOR<sup>1,4</sup>, ANDREW SCHECHTMAN-ROOK<sup>1,5</sup>, PAUL HARDING<sup>1</sup>, LUCA CASAGRANDE<sup>6</sup>, CONSTANCE ROCKOSI<sup>7</sup>, BRIAN YANNY<sup>8</sup>, TIMOTHY C. BEERS<sup>9,10</sup>, JENNIFER A. JOHNSON<sup>11</sup>, DONALD P. SCHNEIDER<sup>12,13</sup>

<sup>1</sup> Department of Astronomy, Case Western Reserve University, Cleveland, OH 44106

<sup>2</sup> Department of Physics, Grove City College, 100 Campus Dr., Grove City, PA 16127

<sup>3</sup> Department of Science Education, Ewha Womans University, Seoul 120-750, Republic of Korea

<sup>4</sup> Department of Physics and Astronomy, Michigan State University, 567 Wilson Rd, East Lansing, MI 48824

<sup>5</sup> Department of Astronomy, University of Wisconsin, 475 North Charter Street, Madison, WI 53706

<sup>6</sup> Research School of Astronomy and Astrophysics, Mount Stromlo Observatory, The Australian National University, ACT 2611, Australia

<sup>7</sup> UCO/Lick Observatory, University of California, Santa Cruz, 1156 High St., Santa Cruz, CA 95064, USA.

<sup>8</sup> Fermi National Accelerator Laboratory, PO Box 500, Batavia IL 60510, USA

<sup>9</sup> Department of Physics, University of Notre Dame, 225 Nieuwland Science Hall, Notre Dame, IN 46656, USA

<sup>10</sup> JINA: Joint Institute for Nuclear Astrophysics, University of Notre Dame, Notre Dame, IN 46556

<sup>11</sup> Department of Astronomy, Ohio State University, 140 West 18th Avenue, Columbus, OH 43210, USA.

<sup>12</sup> Department of Astronomy and Astrophysics, The Pennsylvania State University, University Park, PA 16802 and

<sup>13</sup> Institute for Gravitation and the Cosmos, The Pennsylvania State University, University Park, PA 16802

*Draft version November 16, 2021*

### ABSTRACT

We present *griz* observations for the clusters M92, M13 and NGC 6791 and *gr* photometry for M71, Be 29 and NGC 7789. In addition we present new membership identifications for all these clusters, which have been observed spectroscopically as calibrators for the SDSS/SEGUE survey; this paper focuses in particular on the red giant branch stars in the clusters. In a number of cases, these giants were too bright to be observed in the normal SDSS survey operations, and we describe the procedure used to obtain spectra for these stars. For M71, also present a new variable reddening map and a new fiducial for the *gr* giant branch. For NGC 7789, we derived a transformation from  $T_{\text{eff}}$  to  $g - r$  for giants of near solar abundance, using IRFM  $T_{\text{eff}}$  measures of stars with good *ugriz* and 2MASS photometry and SEGUE spectra. The result of our analysis is a robust list of known cluster members with correctly dereddened and (if needed) transformed *gr* photometry for crucial calibration efforts for SDSS and SEGUE.

*Keywords:* globular clusters: individual, open clusters and associations: individual

### 1. INTRODUCTION

Calibrations which relate observables such as stellar photometry and spectroscopy to fundamental stellar parameters are a vital part of any survey. The Sloan Digital Sky Survey (SDSS: York et al. 2000) provided imaging in five passbands (*ugriz*) for 14,555 square degrees of the sky, using a dedicated imager (Gunn et al. 1998) on the SDSS 2.5m telescope (Gunn et al. 2006). This photometric database was complemented by spectroscopic observations using a multi-object spectrograph (Smee et al. 2013). The original purpose of the SDSS survey was to map the extragalactic universe by obtaining spectra of one million galaxies and one hundred thousand quasars. However, because of a number of important, serendipitous discoveries on the Milky Way, two surveys (SEGUE-1 and -2) which focused on the stellar populations in the Milky Way were carried out as extensions to the original SDSS. SEGUE-1 (Yanny et al. 2009) acquired data from 2005 through 2008, and SEGUE-2 (Eisenstein et al. 2011, Rockosi et al., in preparation) in 2008 and 2009.

Because the SDSS *ugriz* photometric system (Fukugita et al. 1996) was originally designed for the study of galaxies and quasars rather than stars (focusing on avoiding strong sky lines rather than on features in a zero redshift stellar spectrum), one of the important tasks for the SEGUE survey was to obtain observations in *ugriz* for well-studied objects with

known stellar parameters. This program has allowed us to understand how  $T_{\text{eff}}$ ,  $\log g$  and  $[\text{Fe}/\text{H}]$  map into the SDSS colors. Such understanding is particularly important when studying stars from minority populations in the Galaxy such as its halo, as there are often  $[\text{Fe}/\text{H}]$  and luminosity terms in transformations from other photometric systems to *ugriz*, particularly in the *u* and *g* filters (for example, see Figure 10 of Yanny et al. 2009). Open and globular clusters are particularly suitable as calibrators because they provide many objects with the same values of  $[\text{Fe}/\text{H}]$ .

The first order of business in using star clusters is to obtain a good color-magnitude diagram (CMD) in the appropriate filter set. Because the SDSS photometric pipeline (Stoughton et al. 2002) does not perform well in crowded fields, An et al. (2008) performed DAOPHOT photometry of open and globular clusters imaged by SDSS. An et al. (2008) then provided accurate fiducial sequences for 17 globular and 3 open clusters covering a metallicity range from  $[\text{Fe}/\text{H}] = -2.4$  to  $+0.4$ . However, since the SDSS camera saturates at around  $g = 14.5$ , and a number of these clusters have giant branches reaching significantly brighter than this limit, it was necessary to use observations from other telescopes. The *u'g'r'i'z'* system is defined by the same filters as the *ugriz* system and was intended to simplify observations in *ugriz* from other telescopes (Smith et al.

2002; Tucker et al. 2006). However, because the filters are in vacuum in the SDSS imager but not when used in other telescopes, the two photometric systems are in fact different. We used the  $u'g'r'i'z'$  observations of the bright giant branches of these clusters (Clem et al. 2008), transforming them to  $ugriz$  using the transformations of Tucker et al. (2006).

The next step in the use of clusters as calibrators is to make sure that the stars we study are in fact cluster members. Spectroscopic observations provide velocities and other useful discriminants of membership, and the SEGUE survey obtained spectra of stars in 13 clusters (Lee et al. 2008b; Smolinski et al. 2011). These two papers used velocity, position on the CMD and the metallicity of the star as measured by the SEGUE Stellar Parameters Pipeline (SSPP; Lee et al. (2008a,b); Allende Prieto et al. (2008); Smolinski et al. (2011)) as membership criteria.

Our particular interest is the cluster red giant branches. For technical reasons described below, the giant branch stars were not well covered in the previous tests of the SSPP by Lee et al. (2008b) and Smolinski et al. (2011). The next paper in this series (Morrison et al 2015, in preparation) shows how we used the clusters described in this paper to test the values of  $[\text{Fe}/\text{H}]$  and  $\log g$  for cluster members, and adds an additional luminosity discriminant (the Mg index) to enhance the SSPP's ability to identify red giant stars. A number of the clusters described here either have low radial velocities or are located at low galactic latitude, making it difficult to distinguish cluster members from foreground disk stars using only velocity. We have chosen to identify cluster members using a different set of criteria than Lee et al. (2008b) and Smolinski et al. (2011): while we both use the SEGUE velocities and the position on the cluster CMD, we have chosen not to use the SSPP metallicity, and have added another powerful discriminant: the stellar proper motion. Proper motion data are available for all but one clusters we study. In one particularly recalcitrant case, Berkeley 29, where proper motions were not available, we used the velocity and CMD criteria, then rejected foreground dwarfs by visual inspection of the spectra.

M71 is a particularly important and difficult case. It is the only well-studied, nearby cluster with an intermediate metallicity which is accessible from the Northern Hemisphere. Unfortunately, it also has variable reddening across its face. Thus we needed to derive individual reddening estimates for different regions of the cluster (using the photometry of Clem et al. 2008) before we could produce a cluster CMD suitable for producing a fiducial for the giant branch.

In this paper we present, for each cluster, a CMD showing the stars which are likely members and were observed spectroscopically by SEGUE, and a table of accurate coordinates and other information on these likely cluster members. We also describe the SEGUE observations of cluster stars when the cluster focal plane fiber plug-plates (plates hereafter) differed in observational procedure from the usual survey plates. In addition we provide a table of our derived spatial reddening offsets for M71 and a transformation between  $T_{\text{eff}}$  and  $g-r$  for near solar abundance giants.

## 2. CLUSTERS USED FOR CALIBRATION

The SEGUE project observed a number of globular and open clusters for calibration purposes. For calibration of the red giants, we selected the globular clusters M92, M13 and M71 (spanning metallicities from  $-2.4$  to  $-0.8$ ) and the open clusters Be 29, NGC 7789 and NGC 6791, whose  $[\text{Fe}/\text{H}]$  values range from  $-0.4$  to  $+0.4$ . In all but one case, the clusters are within the SDSS footprint and so  $ugriz$  photometry is available for the cluster stars.

The SDSS cluster images were analyzed using DAOPHOT (Stetson 1987) by An et al. (2008) because the SDSS photometric pipeline was not designed to handle crowded fields. However, in most cases the cluster giant branch stars were too bright to be observed in the standard  $ugriz$  system (defined by the data taken on the SDSS 2.5m) because they are saturated in the SDSS exposures. In these cases we used the  $u'g'r'i'z'$  photometry described in Clem et al. (2008), transforming using the equations of Tucker et al. (2006). An et al. (2008) checked these transformations using data available in both  $ugriz$  and  $u'g'r'i'z'$  and found agreement at better than the 2% level for all clusters except NGC 6791, where stars at the tip of the giant branch were redder in standard  $ugriz$  than in transformed  $u'g'r'i'z'$  by 0.05 to 0.10 magnitudes. This discrepancy becomes particularly significant redder than  $g-r=1.0$ . Fortunately, NGC 6791 is sufficiently distant that we are able to use the SDSS  $ugriz$  for all its red giants.

We summarize the values of distance modulus,  $[\text{Fe}/\text{H}]$  and  $E(B-V)$  that we adopted for these clusters, along with the sources of these measurements, in Table 1. For the globular clusters we use the metallicity scale of Kraft & Ivans (2003), based on FeII lines.

In addition, we checked the list of globular cluster variables compiled by Christine Clement<sup>1</sup> to see if any of the stars that we observed were long-period variables, since their use as calibrators would be unwise. We found that there were no known LPVs in our sample of globular cluster stars.

The SEGUE-1 survey is described in Yanny et al. (2009). The survey obtained low-resolution ( $R\sim 1800$ ) spectra for the wavelength region from 3800 to 9000 Å. Each spectroscopic pointing had a bright and faint plug-plate (plate hereafter), with exposure times of typically one and two hours respectively. This procedure allowed us to reduce the effect of scattered light from bright stars in adjacent fibers to fainter stars by limiting the magnitude range on a given plate. For the clusters, we used a more flexible setup to attempt to obtain spectra with good S/N for as many stars as possible.

For many clusters, more than one plate was designed and observed. Table 2 summarizes the information on the plates taken for each cluster discussed in this paper; often a cluster had both a bright and a faint plate designed. For the brightest stars in M92 and M13, only a very short exposure, of duration 1-2 minutes, was needed. This caused a possible problem with our spectroscopic reduction pipeline, since it uses night sky lines in the spectra to check the wavelength calibration, and such short exposures are too short to properly expose the sky lines. We evolved the following procedure in order to

<sup>1</sup> found at <http://www.astro.utoronto.ca/~cclement/read.html>

make such observations process correctly in the pipeline. The brightest stars were observed by drilling their fiber holes on the bright plate at a position offset by 0.02 degrees in RA ( $\cos(\text{Dec})^{-1}$ ). This offset is  $\sim 1.5$  arcmin for M92 and M13. While the rest of the stars on the bright plate were observed, a sky spectrum accumulated in these fibers. When the bright exposure was finished, the telescope was moved by this offset, taking the regular stars away from their fibers and placing the brightest stars on the fibers which had been accumulating sky photons. The plate was then exposed for an additional short time. The coordinates in the SDSS database have been corrected for these offsets. The referee has asked whether starlight could have accumulated in these offset fibers during the ‘sky’ exposures. We note that we avoided placing fibers on the bright central regions of both clusters, with the nearest star more than  $2'$  from the cluster center in M92 and  $\sim 1'$  from the less crowded center of M13. Thus it is unlikely that any light from cluster stars will contaminate the M92 offset fibers, and a little more likely for M13, where we note that in some of the stars observed with offsets, the signal-to-noise ratio is lower than expected at the blue end of the spectrum ( $4000\text{\AA}$  and below).

In addition, this offset procedure may introduce additional uncertainties on the radial velocities. Yanny et al. (2009) quantify the radial velocity uncertainty for SEGUE survey plates as a function of both  $g$  magnitude and S/N. The CMDs of the clusters in the following section show that SEGUE observed stars as faint as  $g=20$ , with a wide range of  $g-r$  color. At magnitudes greater than  $g=19$ , velocity errors can be  $20\text{ km s}^{-1}$  or more. However, the red giants in the clusters, the major object of this paper, are redder and in general much brighter. For all clusters except Be 29, the giants have  $g < 16$ , which give radial velocity errors around  $5\text{ km s}^{-1}$  for the red giants. Be 29’s giants can be as faint as 19, and so we expect larger velocity errors for this cluster of up to  $10\text{ km s}^{-1}$ . The two clusters with offset observations (M92 and M13) may have an additional error of a few  $\text{km s}^{-1}$  introduced for the brightest stars.

The spectroscopic observations of the near solar metallicity open cluster NGC 7789 were targeted on the giant branch only, because there are already good SEGUE spectroscopic observations of stars below the main-sequence turnoff in two open clusters with  $[\text{Fe}/\text{H}]$  close to solar: M67 and NGC 2420.

### 3. CLUSTERS WITH PROPER MOTION DATA

We used the proper motions of Cudworth and collaborators for M92, M13, M71 (Rees 1992; Cudworth & Monet 1979; Cudworth 1985, respectively) and for NGC 6791 (Cudworth, private communication). For NGC 7789 we used the proper motions of McNamara & Solomon (1981).

Because the radial velocity zeropoint was uncertain for some of the brighter cluster plates, we first examined the proper motion members (those with membership probability greater than 70%) to obtain a clean radial velocity distribution for the cluster. We then used this to find the optimal range of radial velocities for cluster membership selection.

#### 3.1. M92

For the most metal-poor globular cluster in our dataset, M92, the giant branch tip is at  $r \sim 11.5$ , so most of the red giant branch is saturated in the SDSS photometry. We therefore used both the  $ugriz$  photometry of An et al. (2008) (reference run 4682 plus run 5237, transformed to the reference frame using the transformations given in An et al. (2008)) and the transformed photometry of Clem et al. (2008) to construct the color-magnitude diagram (Figure 1).

SDSS photometric reductions have improved over the years of the survey. An important advance occurred between Data Releases (DR) 7 and 8: what is known as the ‘‘Ubercalibration’’ (Padmanabhan et al. 2008). This technique solves for the photometric calibration parameters using all overlapping observations. When An et al. (2008) first made the DAOPHOT reductions of the cluster data available, they calibrated these reductions to DR7. Subsequently, An et al. (2013) calculated the offsets to apply in order to put the cluster photometry on the DR8 system, and we have applied these offsets to the An et al. photometry given in Table 3.

Proper motions from Rees (1992) are available for all giants above the level of the horizontal branch. We chose a radial velocity range of  $-123$  to  $-103\text{ km s}^{-1}$  for cluster members. Coordinates,  $griz$  photometry and its source, SEGUE radial velocities and proper motion membership probabilities for each member are given in Table 3.

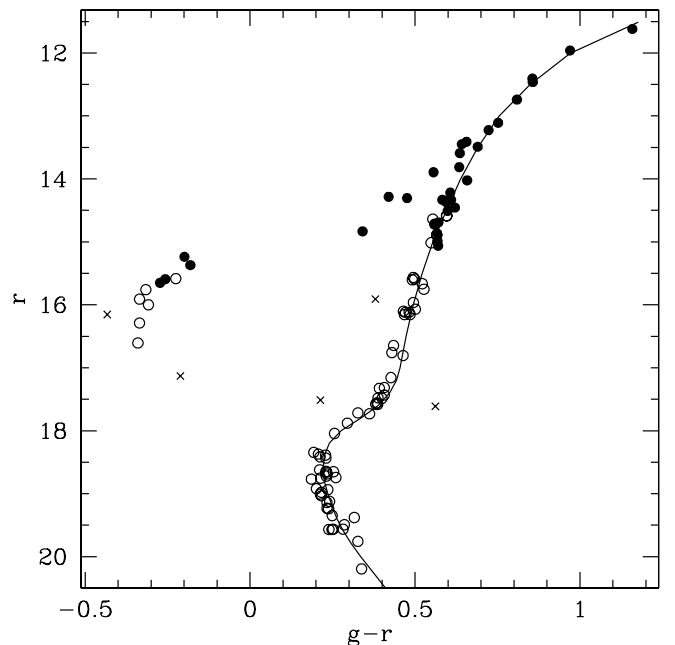


**Figure 1.**  $gr$  CMD of the globular cluster M92, using data from An et al. (2008) and Clem et al. (2008). All points plotted are radial velocity members. Stars with proper motion membership probabilities higher than 70% are shown as filled circles, while stars with no proper motions available are shown with open circles. Crosses are stars which are classified as non-members because of their position in the CMD. The solid line is the fiducial of Clem et al. (2008), transformed to  $gr$  using the transformation of Tucker et al. (2006).

#### 3.2. M13



M13 also has bright giants, so the color-magnitude diagram shown in Figure 2 uses photometry from both An et al. (2008) and Clem et al. (2008). For the photometry from An et al. (2008), we used runs 3225 and 3226, correcting run 3226 to the reference run (3225) using the corrections given in An et al. (2008), and then applied the ‘‘Ubercalibration’’ corrections given in Table 1 of An et al. (2013). We chose a radial velocity range of  $-251$  to  $-239$   $\text{km s}^{-1}$  to select radial velocity members for this cluster. Proper motions are available for all of the stars on the giant branch above the horizontal branch.

Data on individual cluster members are given in Table 4.

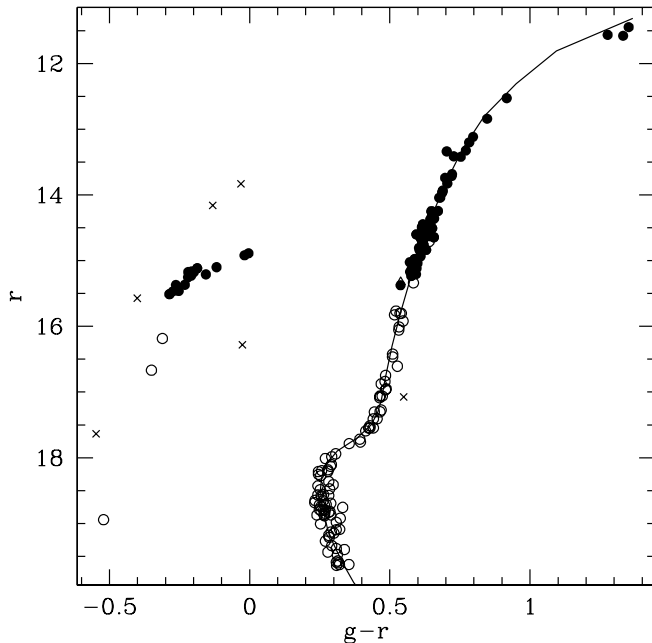


**Figure 2.**  $gr$  CMD of the globular cluster M13, using data from An et al. (2008) and Clem et al. (2008). All points plotted are radial velocity members. Symbols have the same meaning as in Figure 1. The solid line shows the transformed fiducial of Clem et al. (2008).

### 3.3. M71

Unlike the two globular clusters previously discussed, M71 is a disk globular cluster in a low-latitude field with variable reddening (see, e.g. Casagrande et al. 2010). However, it is one of the few clusters in this metallicity range accessible from the North. Its low galactic latitude makes membership decisions more difficult because of the large number of foreground disk stars. In addition, M71’s radial velocity is closer to that of the field stars because of its disk-like orbit: the difference is only  $\sim -20$   $\text{km s}^{-1}$ , compared to the M92 and M13 radial velocities which are  $100$   $\text{km s}^{-1}$  (or more) different from the field star radial velocities.

Comparison of the giant branch fiducial of Clem et al. (2008) for M71 with other cluster fiducials suggests that the shape of the Clem et al. (2008) fiducial is slightly incorrect, presumably because of the larger probability of field star contamination on M71’s giant branch, and because even genuine members have variable reddening and

thus they do not trace a tight fiducial. We have therefore constructed a new fiducial for the M71 giant branch in  $g$  and  $r$ , using only stars which are likely members, and have tightened up the CMD by estimating the variable reddening across M71’s field, using the position of the main sequence turnoff in Clem’s accurate photometry.

To construct the CMD for M71 using likely members only, we started with stars which had more than a 70% probability of membership from the proper motions of Cudworth (1985) and from unpublished data kindly made available by Kyle Cudworth for the fainter stars. These data reach more than a magnitude below the horizontal branch, so are ideal for our purposes. We use the photometry of Clem et al. (2008), converted to  $gr$  using the transformations in Tucker et al. (2006).

For radial velocity membership data, in light of the small difference between M71’s velocity and that of contaminating field stars, a more accurate velocity catalog was extremely helpful: Tad Pryor (private communication) kindly provided unpublished velocity data for almost all stars on or above the horizontal branch in M71. These data were obtained with high-resolution spectrographs on the DAO 48-inch and the KPNO 4m and have errors  $\leq 1$   $\text{km s}^{-1}$ . There were also multiple observations for many of the stars, allowing likely binaries to be flagged via their radial velocity variability. The higher velocity accuracy allowed us to use a narrower window to define velocity membership:  $-20$  to  $-27$   $\text{km s}^{-1}$ . We also rejected one star with both radial velocity and proper motion suggesting membership (star 1-1, on plate/MJD/fiber 2333/53682/165) but with radial velocity variations which may be due to binarity.

To estimate variable reddening values across the field of M71, we used the M71 photometry of Clem et al. (2008) to map the position of the main sequence turnoff across the field, using  $g-i$  to provide a more sensitive measurement. We divided the region near M71 into square regions of size  $50$  arcsec, plotted the CMD near the turnoff for each region, and then overlaid the Clem et al. (2008) M71 fiducial, varying the reddening offset by eye until we obtained the best fit. The scatter around the fitted fiducial gives an estimate of the remaining variation in reddening inside the  $50$  arcmin square field (because the Clem et al photometry was internally accurate to significantly better than  $0.01$  mag. at these bright magnitudes). This scatter had a range of  $0.020$  to  $0.075$  in  $g-i$  around the fiducial (equivalent to up to  $0.05$  in  $E(g-r)$ ). Our reddening offsets are given in Table 6 and vary between  $+0.07$  and  $-0.03$  in  $E(B-V)$  over the M71 field, which is  $9.2$  arcmin on a side.

Applying these reddening offsets to the confirmed cluster members (and using the global reddening and distance modulus values given in Table 1) results in the CMD shown in Figure 3, which can be compared with Figure 12 of Clem et al. (2008). (We used Clem’s photometry in this case because the stars on M71’s giant branch were either saturated or close to saturated in the original SDSS exposure.) Our CMD is significantly cleaner, with foreground stars removed and the red giant branch, red horizontal branch (RHB) and asymptotic giant branch more clearly visible. Likely AGB stars are circled in magenta in the Figure: there are 11 of them. We show our improved fiducial for the M71 giant branch in the Figure. This fiducial is tabulated in Xue et al.

(2014).

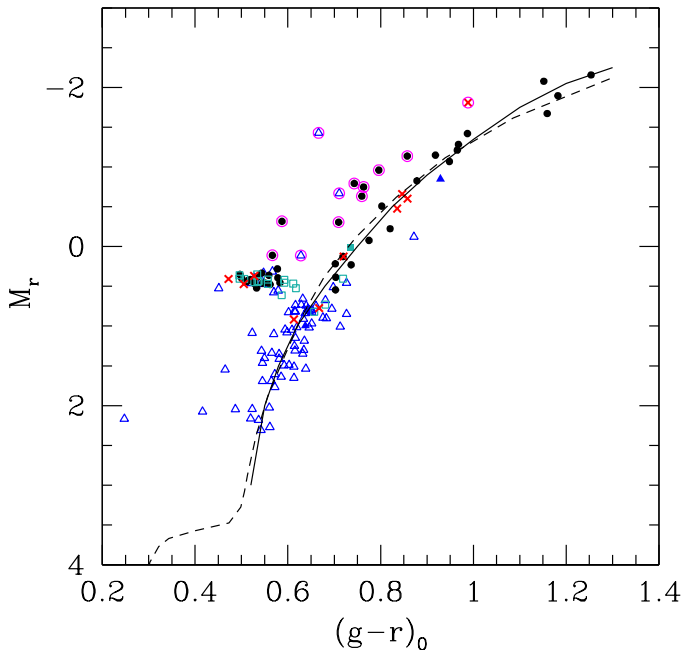


**Figure 3.** CMD of the globular cluster M71, using data from Clem et al. (2008) transformed to  $gr$  using the transformations of Tucker et al. (2006). Only stars with more than a 70% probability of proper motion membership are plotted. Solid symbols denote stars where variable reddenings have been estimated and applied, while open symbols use  $E(B-V)=0.28$ . Black circles show stars with multiple radial velocity observations that are radial velocity members without variable velocities. Red crosses show stars with radial velocity variability suggesting that the star may be part of a binary system or a long-period variable. Blue/green squares indicate stars with one radial velocity measurement which are velocity members. Likely AGB stars are marked with a large magenta circle. Blue triangles denote stars without radial velocity measurements. The solid black line traces our new M71 giant branch fiducial, and the dotted line the Clem et al. (2008) fiducial.

Table 5 lists our cluster members for M71. We also list the unpublished velocities of Pryor and collaborators, our adopted reddening offsets in  $E(B-V)$  for each of these stars, and the ID of each star from Cudworth (1985) in order to make comparison with other studies easier. Figure 4 shows the confirmed members that were observed by SEGUE on M71’s CMD. We have chosen to show two CMDs for M71 because showing the stars with spectroscopic observations in Figure 3 would detract from the membership information and the new fiducial presented there.

### 3.4. NCG 7789

NGC 7789 is a populous open cluster with a metal abundance slightly less than solar (Tautvaišienė et al. 2005) and age around 2 Gyr (Gim et al. 1998b). We selected targets using proper motion information from McNamara & Solomon (1981) and velocities from Gim et al. (1998a). Our selected members have SEGUE radial velocities between  $-51.5$  and  $-48.2$  km s $^{-1}$ . Figure 5 shows the radial velocities of stars in the SEGUE plate which observed NGC 7789, and illustrates some of the problems of obtaining reliable member lists for open

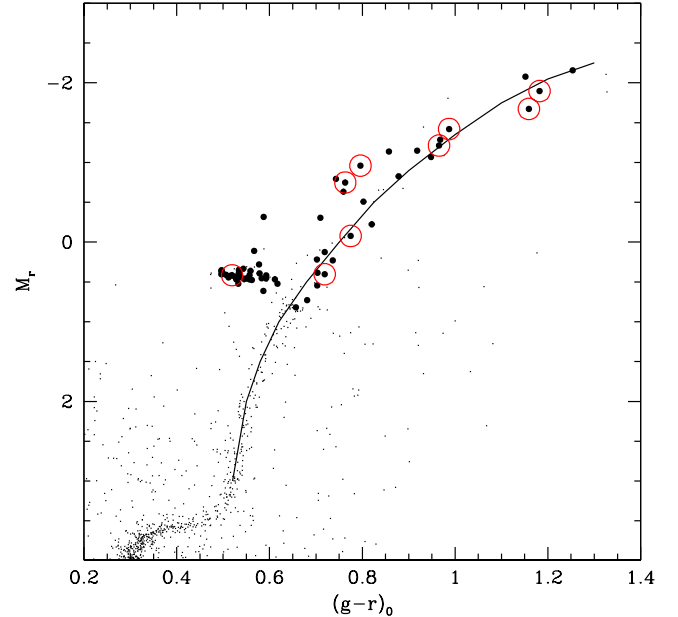


**Figure 4.** CMD of the globular cluster M71, using data from Clem et al. (2008). Stars without velocity data are shown as small black dots, while stars with proper motions and radial velocities indicating membership are shown as large black dots. Stars observed by SEGUE are shown by large red circles.

clusters. All of the stars we targeted as likely giants are in the largest peak in the histogram, centered on  $-50$  km s $^{-1}$ , but the contribution of foreground and background disk stars to the velocity histogram, even at the exact cluster velocity, is significant.

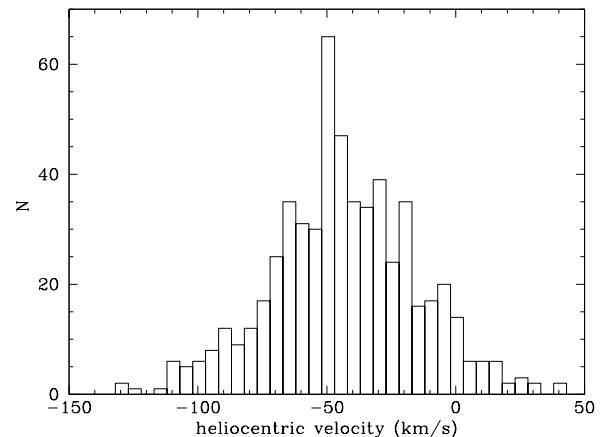


**Figure 5.** Velocity histogram of stars on the NGC 7789 plate. The broad spread of velocities from foreground/background disk stars is clear. All our targeted members are in the highest peak at  $-50$  km s $^{-1}$ , but roughly half the stars in this bin are still likely to be field stars.

To produce our membership list, we rejected four of the stars which were both proper motion and velocity members because of their position in the color-magnitude diagram shown in Figure 6. While these stars may be members whose variable reddening moves them away from the cluster sequence, we have chosen to be conservative and reject them, since a major aim of this paper is sim-

ply to produce a collection of cluster stars which have a high likelihood of being members. We also rejected one star because (Gim et al. 1998a) noted that it had radial velocity variations.

Since there are no *ugriz* data available for NGC 7789, we show *V* and *I* photometry from Gim et al. (1998b) in the color-magnitude diagram of Figure 6, with the cluster members observed by SEGUE highlighted. The large contribution from foreground/background disk stars is clear in the CMD as well. The variable reddening can be seen in the scatter of colors and magnitudes in the clump in particular. Individual estimates of reddening values were available for about one-third of the giants from the Vilnius photometry of Bartašūtė & Tautvaišienė (2004). We used these values where available, and their cluster value ( $E(B - V) = 0.25$ ) otherwise.

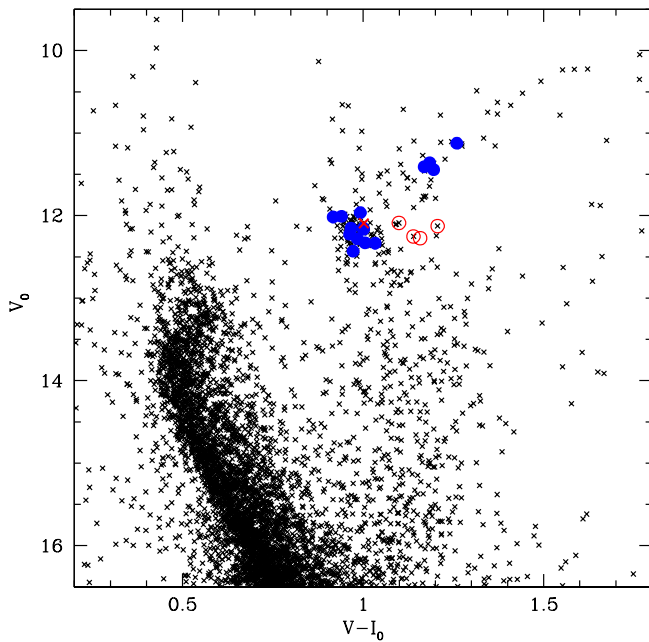


**Figure 6.** VI CMD of the open cluster NGC 7789, based on data from Gim et al. (1998b). Stars which are proper motion, radial velocity (from SEGUE) and CMD members are shown as filled blue circles. Stars which are proper motion and radial velocity members which we chose to reject because of their position on the CMD are shown with red open circles, while the star which Gim et al. (1998a) note has radial velocity variations is shown with a red cross.

Since there are no *ugriz* or *u'g'r'i'z'* data available for this cluster, we transformed from  $V - K_s$  to  $g - r$  via  $T_{\text{eff}}$  measurements. First, we used the relation between  $V - K_s$  and  $T_{\text{eff}}$  of Ramírez & Meléndez (2005), the *V* magnitudes of Gim et al. (1998b), 2MASS *K* magnitudes and  $E(B - V)$  to derive  $T_{\text{eff}}$  for each star. We chose to use  $V - K_s$  because its relation between effective temperature and color is the least sensitive to  $[\text{Fe}/\text{H}]$  and gravity (Bessell 2008). We then derived a relation between  $T_{\text{eff}}$  and  $g - r$  using the Infrared Flux Method (IRFM hereafter) colors of stars observed with SEGUE which had near-solar abundances. We selected 2068 stars with SDSS spectra, good *ugriz*, 2MASS *J*, *H* and *K\_s* colors, SPP metallicities between  $-0.2$

and  $+0.25$  (which have a mean metallicity of  $-0.05$ , the same as NGC 7789) and low reddening:  $E(B - V)$  from Schlegel et al. (1998) less than 0.025. Casagrande et al. (in preparation) computed individual Infrared Flux Method (see Blackwell & Shallis 1977; Casagrande et al. 2010) temperatures for a large number of stars observed by SEGUE, including these stars. Figure 7 shows the relationship between  $(g - r)_0$  and this IRFM  $T_{\text{eff}}$  for all stars with low reddening (blue points) and for stars with near solar abundance (red points). We fitted cubic relationships to these low-reddening, near solar abundance stars as follows, first defining  $Q = 5040/T_{\text{eff}}$ .

$$Q = 0.6728 + 0.4265 (g - r)_0 + 0.08841 (g - r)_0^2 - 0.08881 (g - r)_0^3 \quad (1)$$

The differences between this line and the actual  $T_{\text{eff}}$  values have a sigma of 112 K.

The inverse relation is:

$$(g - r)_0 = -0.3672 - 0.7188 Q + 2.281 Q^2 - 0.4688 Q^3 \quad (2)$$

The differences between the fit line and the actual  $(g - r)_0$  values is 0.047 mag. Assuming errors of 0.02 mag. for the *V* and  $K_s$  magnitudes gives a random error estimate of 0.055 mag. for this entire process. Lastly, we added 100K to the  $T_{\text{eff}}$  from Ramírez & Meléndez (2005) to correct for the difference in absolute scale between their IRFM scale and that used by Casagrande et al. (see Casagrande et al. 2010, for a detailed discussion of this point) then used equation (2) to calculate the value of  $(g - r)_0$  for each star.

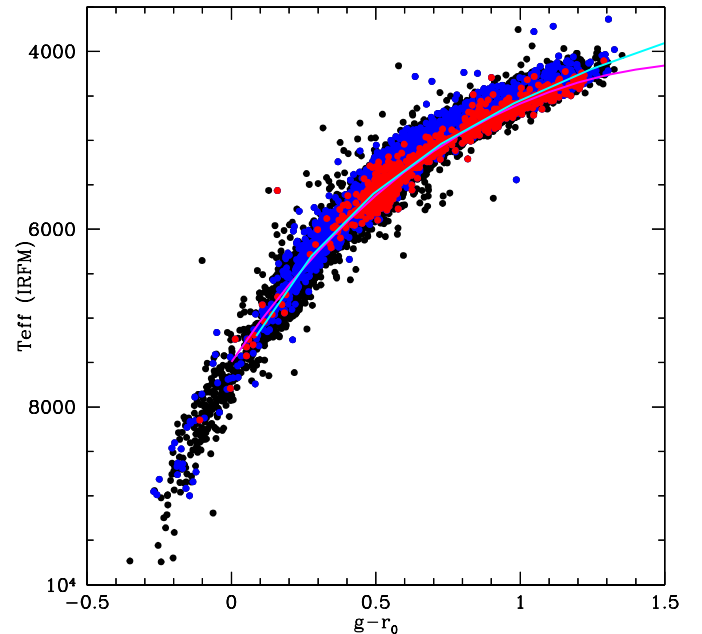


**Figure 7.**  $(g - r)_0$  vs  $T_{\text{eff}}$  calculated using the IRFM for stars with good *ugriz* photometry and good 2MASS colors. Black points show all stars, while blue points show stars with  $E(B - V) < 0.025$ , and red points show the data used to obtain the transformation between  $T_{\text{eff}}$  and  $(g - r)_0$  for stars near solar metallicity, which have the additional restriction of  $-0.2 < [\text{Fe}/\text{H}] < 0.25$  and  $(g - r)_0 > 0$ . Fit lines for equations (1) and (2) are shown with cyan and magenta lines respectively.

We checked this transformation using an open clus-

ter which has a similar age and metallicity to NGC 7789 but also has  $g'r'$  observations (Platais et al. 2013), NGC 6819. We used the standard transformations of Tucker et al. (2006) to transform the NGC 6819 photometry into  $g$  and  $r$ , and the cluster reddening of  $E(B-V)=0.16$  (Anthony-Twarog et al. 2014), to make the CMD shown in Figure 8. Our 15 confirmed NGC 7789 red giants and clump stars are overplotted. The solid blue symbols are proper motion members of NGC 6819, while the red crosses are our NGC 7789 members. Since there are a range of cluster distance moduli for NGC 6819 in the literature, we adjusted the NGC 6819 absolute magnitudes until the clumps of the two clusters coincided. The agreement of  $g-r$  color between the two clumps is gratifying, suggesting that our transformation from VI to  $g-r$  is quite accurate.

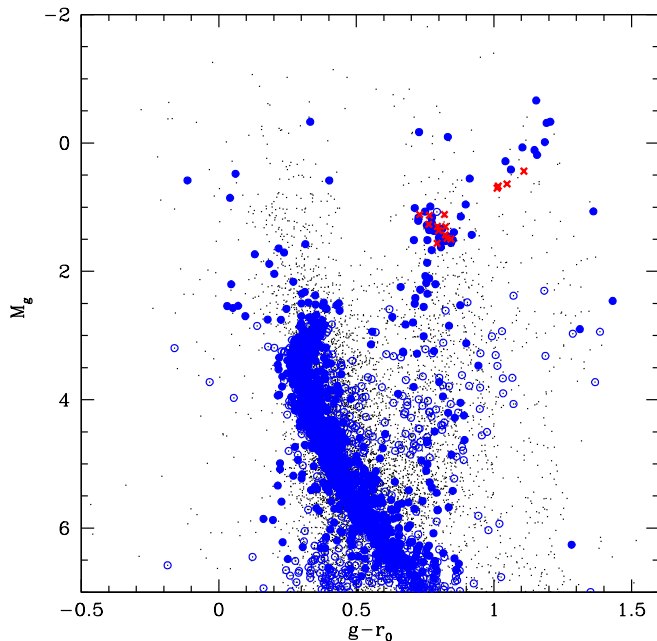


**Figure 8.** CMD of NGC 6819, a near ‘twin’ of NGC 7789, with photometry from Platais et al. (2013). Small black points show all stars in the field, open blue circles are stars with proper motion membership probability (from Platais et al. 2013) greater than 50%, and closed blue circles stars with membership probabilities greater than 80%. Red crosses show our NGC 7789 members. The close agreement in clump star colors indicates that our transformation from VI to  $gr$  for NGC 7789 stars is quite accurate.

Data on NGC 7789 members are listed in Table 7. The  $V$  and  $I$  photometry are from Gim et al. (1998b), radial velocities from our SEGUE data and reddening values from Bartašūtė & Tautvaišienė (2004), and  $(g-r)_0$  values from the transformation described above.

### 3.5. NGC 6791

NGC 6791 is a particularly useful cluster because it anchors our calibrations at the metal-rich end, having  $[Fe/H] = +0.39$ . We used run 5416 of the photometry from An et al. (2008) and applied the ‘ubercalibration’ corrections given in Table 1 of An et al. (2013). To determine membership we used proper motion data from Cudworth (private communication), choosing all stars with

proper motion membership probability greater than 70%, velocities between  $-60$  and  $-48$   $\text{km s}^{-1}$ , and finally, by removing several stars whose position on the CMD was not consistent with membership of the cluster. We remind the reader that our aim here is to obtain a collection of the most likely cluster members, not a complete set, and such rejection is a conservative step for this purpose. Figure 9 shows the NGC 6791 stars observed by SEGUE on the cluster CMD, and Table 8 lists the likely members of the cluster.

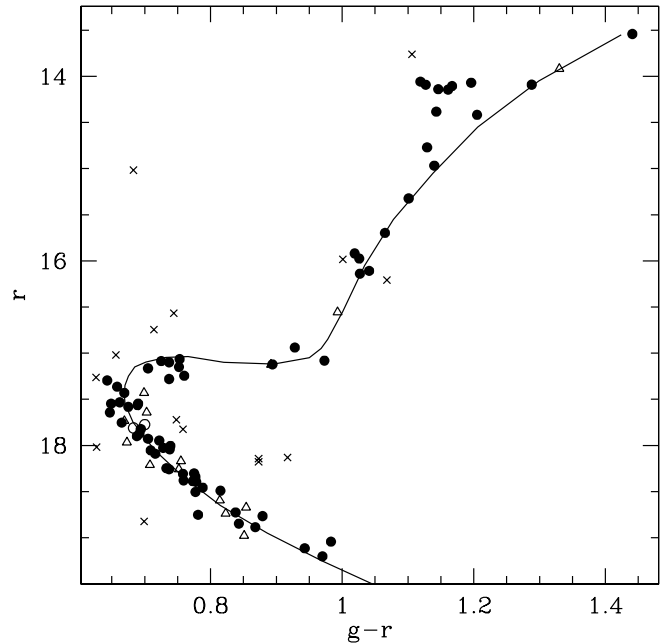


**Figure 9.**  $gr$  CMD of the rich open cluster NGC 6791, using data from An et al. (2008). Circles and triangles show radial velocity members. Stars with proper motion membership probabilities higher than 70% are shown as filled circles, while those with proper motion membership probabilities smaller than 70% are shown with open triangles. If no proper motion is available for the star, it is shown with an open circle. Crosses show stars classified as non-members because of their position in the CMD.

## 4. A CLUSTER WITH NO PROPER-MOTION DATA: BERKELEY 29

Useful proper motion data are not available for the open cluster Be 29. However, the cluster was observed using the SDSS imager on the 2.5m telescope at the end of the SDSS-III imaging season in Jan 2009 (Aihara et al. 2011), and we include its  $gr$  photometry in this work. Following the procedure in An et al. (2008) used for the other SDSS clusters, we reduced SDSS imaging frames using the DAOPHOT/ALLFRAME suite of programs (Stetson 1987; Stetson 1994), and converted DAOPHOT magnitudes into the SDSS asinh values (Lupton et al. 1999) using photometric zero points, extinction coefficients, and airmass values. We tied our cluster photometry to the ubercal system, as for the other cluster photometry discussed in Section 3, by deriving zero-point offsets between DAOPHOT and DR8 photometry in low density fields near Be 29. We checked the adjusted DAOPHOT magnitudes in these cluster flanking fields with more recent values in DR12 (Alam et al. 2015),



and found 0.008 mag differences in each of the  $g$  and  $r$  passbands. The  $gr$  CMD of Be 29 is shown in Figure 7: the red clump can be seen near  $g - r = 0.8$  and  $r = 17$ .

Be 29’s stars were in general fainter than those in the other clusters we studied, because we aimed to obtain unsaturated photometry of its giant branch. This led to larger than average velocity errors on the Be 29 stars. Because Be 29’s radial velocity is close to that of the disk stars in the field, contamination from foreground/background disk stars is a problem, and we do not have a very accurate radial velocity to use for member identification. However, as we showed in our discussion of NGC 7789, even full velocity and proper motion data for each star is not sufficient to identify members for open clusters. Our strategy, therefore, was to adopt a wide velocity window (10–40 km s<sup>-1</sup>) and visually inspect the spectra of the stars within this window to determine if they were giants (and thus likely to belong to Be 29) or dwarfs (and so not cluster members given their colors and magnitudes). The criteria we used for this visual inspection included the strengths of the Mgb/H feature near 5170Å, the strengths of the CaI line at 4227Å (both described in detail in Morrison et al. 2003), and the relative strength of the SrII line at 4077Å to the nearby FeI lines at 4045 and 4063Å (Rose 1984).

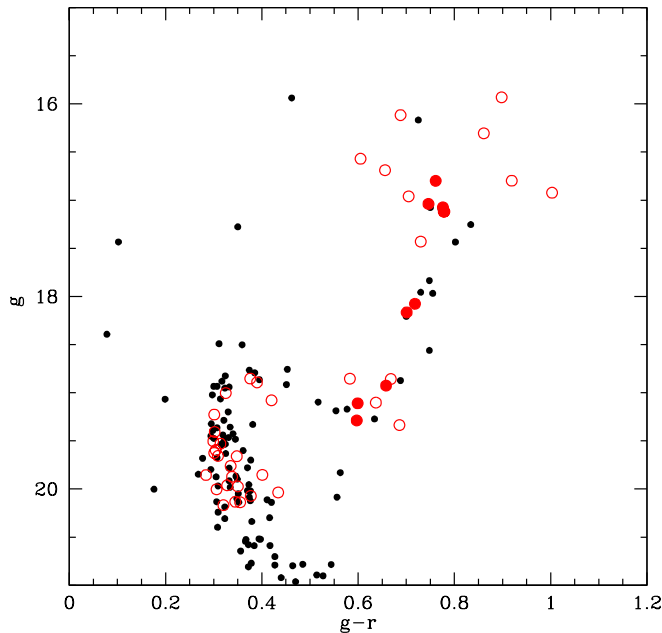


**Figure 10.** CMD of the open cluster Be 29. Filled black circles show stars from the DAOPhot reductions of the SDSS photometry which are within 3 arcmin radius of the cluster center. The most luminous giants in this plot are on the red horizontal branch. Open red circles show radial velocity members in the giant branch color range, while filled red circles show stars confirmed spectroscopically to be giants. It can be seen that there is significant contamination by non-cluster members in the CMD.

Table 9 provides detail on the Be 29 members observed by SEGUE.

## 5. SUMMARY

We present CMDs and membership information for stars from the globular clusters M92, M13 and M71 and the open clusters Berkeley 29, NGC 7789 and NGC 6791.

For the nearby globular clusters M92 and M13 ([Fe/H]=−2.4 and −1.6 respectively), we describe the procedures used to observe the brightest giants spectroscopically on the SDSS 2.5m and the transformation of the  $u'g'r'i'z'$  magnitudes of these bright stars to  $ugriz$ . We used multiple criteria to isolate cluster members: the SEGUE radial velocity, proper motions and CMD position. We tabulate  $griz$  magnitudes and SEGUE radial velocity measures for the 79 M92 members and the 146 M13 members.

In the disk globular cluster M71 ([Fe/H]=−0.8), reddening is variable due to its low galactic latitude. We mapped this variation using the position of the main sequence turnoff in the photometry of Clem et al. (2008) and give a table of variable reddening values for this cluster. The improved reddening estimates produced a much cleaner CMD and allowed us identify possible AGB members and to construct an improved fiducial for the red giant branch, important for our K giant distance estimates. This fiducial is tabulated in Xue et al. (2014). We give  $gr$  photometry, reddening offsets and velocities for the 9 members on the giant or horizontal branch which were observed by SEGUE.

Open clusters are traditionally harder to study because their low galactic latitudes and low concentration lead to large contamination from non-members, even when accurate radial velocity and proper motions are available.

The open cluster Be 29 ([Fe/H]=−0.4) has no proper motion data available, and because its stars are relatively faint, the SEGUE radial velocities have errors of order 10 km s<sup>-1</sup>. Thus we supplemented the velocity and CMD position criteria with a visual inspection of the SEGUE spectra in order to cull out the foreground dwarf stars in the field of this cluster. We tabulate  $gr$  photometry and velocity measurements for the 10 cluster members on the lower giant branch and red clump for this cluster.

The open cluster NGC 7789 ([Fe/H]=0.0) has both radial velocity and proper motion data available, but no  $ugriz$  or  $u'g'r'i'z'$  data. We derived a transformation from V-K to  $gr$  for stars with near-solar abundances via recent  $T_{\text{eff}}$  calibrations of stars with good SDSS photometry and SEGUE spectra. We validated this transformation via CMD comparisons with the very similar open cluster NGC 6819, and give photometry and velocities for the 15 giant branch or red clump members of NGC 7789 observed by SEGUE.

The super-metal-rich cluster NGC 6791 ([Fe/H]=+0.4) has higher concentration than many open clusters, so the combination of CMD position, radial velocity and proper motion is sufficient to identify cluster members. We tabulate  $griz$  photometry and SEGUE velocities for the 67 cluster members observed by SEGUE.

The information presented in this paper will be useful in calibrations and tests of the SEGUE observations, particularly for red giant stars, and will be used in the series of papers titled “The SEGUE K giant survey”. These papers include a detailed description of the technique of identifying K giants in SEGUE data (Morrison et al, in preparation), the calculation of distances for the ~6,000 K giants identified by the survey (Xue et al. 2014), a study of substructure in halo giants out to 100



kpc (Janesh et al. 2015), the study of the radial profile of the halo out to 60 kpc, which also includes an estimate of the (slight) radial metallicity gradient in the halo (Xue et al. 2015) and two papers currently in preparation, one on the halo MDF and its variation with distance, and the other on the  $[\alpha/\text{Fe}]$  ratios of  $\sim 2000$  K giants in the halo.

## 6. ACKNOWLEDGEMENTS

We thank Tad Pryor for kindly sharing his unpublished velocity data for M71 with us, and Bruce Twarog for suggesting that we use NGC 6819 to help transform the NGC 7789 data to *gr*. We also thank the anonymous referee for a very helpful report. This research used the facilities of the Canadian Astronomy Data Centre operated by the National Research Council of Canada with the support of the Canadian Space Agency. This publication also makes use of data products from the Two Micron All Sky Survey, which is a joint project of the University of Massachusetts and the Infrared Processing and Analysis Center/California Institute of Technology, funded by the National Aeronautics and Space Administration and the National Science Foundation. This work was supported in part by the National Science Foundation under Grant No. PHYS-1066293 and the hospitality of the Aspen Center for Physics, and by grants AST-1009886 to HLM and AST-121989 to HLM, PH and CR. TCB acknowledges partial support for this work by grant PHY 08-22648: Physics Frontiers Center/Joint Institute for Nuclear Astrophysics (JINA), awarded by the U.S. National Science Foundation.

Funding for SDSS-III has been provided by the Alfred P. Sloan Foundation, the Participating Institutions, the National Science Foundation, and the U.S. Department of Energy Office of Science. The SDSS-III web site is <http://www.sdss3.org/>. SDSS-III is managed by the Astrophysical Research Consortium for the Participating Institutions of the SDSS-III Collaboration including the University of Arizona, the Brazilian Participation Group, Brookhaven National Laboratory, Carnegie Mellon University, University of Florida, the French Participation Group, the German Participation Group, Harvard University, the Instituto de Astrofísica de Canarias, the Michigan State/Notre Dame/JINA Participation Group, Johns Hopkins University, Lawrence Berkeley National Laboratory, Max Planck Institute for Astrophysics, Max Planck Institute for Extraterrestrial Physics, New Mexico State University, New York University, Ohio State University, Pennsylvania State University, University of Portsmouth, Princeton University, the Spanish Participation Group, University of Tokyo, University of Utah, Vanderbilt University, University of Virginia, University of Washington, and Yale University.

## REFERENCES

- Allende Prieto, C., Sivarani, T., Beers, T. C., et al. 2008, *AJ*, 136, 2070  
 An, D., et al. 2008, *ApJS*, 179, 326  
 An, D., Terndrup, D. M., Pinsonneault, M. H., et al. 2007, *ApJ*, 655, 233  
 An, D., Beers, T. C., Johnson, J. A., et al. 2013, *ApJ*, 763, 65  
 Anthony-Twarog, B. J., Tanner, D., Cracraft, M., & Twarog, B. A. 2006, *AJ*, 131, 461  
 Anthony-Twarog, B. J., Deliyannis, C. P., & Twarog, B. A. 2014, *AJ*, 148, 51  
 Bessell, M. S. 2008, *Mem. Soc. Astron. Italiana*, 79, 317  
 Blackwell, D. E., & Shallis, M. J. 1977, *MNRAS*, 180, 177  
 Brogaard, K., Bruntt, H., Grundahl, F., Clausen, J. V., Frandsen, S., Vandenberg, D. A., & Bedin, L. R. 2011, *A&A*, 525, A2  
 Bartašiūtė, S., & Tautvaišienė, G. 2004, *Ap&SS*, 294, 225  
 Carraro, G., Bresolin, F., Villanova, S., Matteucci, F., Patat, F., & Romaniello, M. 2004, *AJ*, 128, 1676  
 Carraro, G., Villanova, S., Demarque, P., McSwain, M. V., Piotto, G., & Bedin, L. R. 2006, *ApJ*, 643, 1151  
 Carretta, E., et al. 2000, *ApJ*, 533, 215  
 Casagrande, L., Ramírez, I., Meléndez, J., Bessell, M., & Asplund, M. 2010, *A&A*, 512, A54  
 Clem, J. L., Vanden Berg, D. A., & Stetson, P. B. 2008, *AJ*, 135, 682  
 Cudworth, K. M., & Monet, D. G. 1979, *AJ*, 84, 774  
 Cudworth, K. M. 1985, *AJ*, 90, 65  
 Eisenstein, D. J., Weinberg, D. H., Agol, E., et al. 2011, *AJ*, 142, 72  
 Frinchaboy, P. M., Muñoz, R. R., Phelps, R. L., Majewski, S. R., & Kunkel, W. E. 2006, *AJ*, 131, 922  
 Fukugita, M., Ichikawa, T., Gunn, J. E., et al. 1996, *AJ*, 111, 1748  
 Gim, M., Hesser, J. E., McClure, R. D., & Stetson, P. B. 1998, *PASP*, 110, 1172  
 Gim, M., Vandenberg, D. A., Stetson, P. B., Hesser, J. E., & Zurek, D. R. 1998, *PASP*, 110, 1318  
 Gratton, R., Bragaglia, A., Carretta, E., & Tosi, M. 2006, *ApJ*, 642, 462  
 Grundahl, F., Stetson, P. B., & Andersen, M. I. 2002, *A&A*, 395, 481  
 Gunn, J. E., Carr, M., Rockosi, C., et al. 1998, *AJ*, 116, 3040  
 Gunn, J. E., Siegmund, W. A., Mannery, E. J., et al. 2006, *AJ*, 131, 2332  
 Jacobson, H. R., Pilachowski, C. A., & Friel, E. D. 2011, *AJ*, 142, 59  
 Janesh, W., Morrison, H. L., Ma, Z., et al. 2015, submitted to *ApJ*, arXiv:1503.09133  
 Kraft, R. P., & Ivans, I. I. *PASP*, 115, 143  
 Lee, Y. S., Beers, T. C., Sivarani, T., et al. 2008, *AJ*, 136, 2022  
 Lee, Y. S., Beers, T. C., Sivarani, T., et al. 2008, *AJ*, 136, 2050  
 McNamara, B. J., & Solomon, S. 1981, *A&AS*, 43, 337  
 Morrison, H. L., Norris, J., Mateo, M., et al. 2003, *AJ*, 125, 2502  
 Önehag, A., Gustafsson, B., & Korn, A. 2014, *A&A*, 562, A102  
 Padmanabhan, N., Schlegel, D. J., Finkbeiner, D. P., et al. 2008, *ApJ*, 674, 1217  
 Platais, I., Gosnell, N. M., Meibom, S., et al. 2013, *AJ*, 146, 43  
 Perryman, M. A. C., et al. 1997, *A&A*, 323, L49  
 Peterson, R. C., & Green, E. M. 1998, *ApJL*, 502, L39  
 Ramírez, I., & Meléndez, J. 2005, *ApJ*, 626, 465  
 Rees, R. F., Jr. 1992, *AJ*, 103, 1573  
 Rose, J. A. 1984, *AJ*, 89, 1238  
 Schlegel, D. J., Finkbeiner, D. P., & Davis, M. 1998, *ApJ*, 500, 525  
 Sestito, P., Bragaglia, A., Randich, S., et al. 2008, *A&A*, 488, 943  
 Skrutskie, M. F., Cutri, R. M., Stiening, R., et al. 2006, *AJ*, 131, 1163  
 Smee, S. A., Gunn, J. E., Uomoto, A., et al. 2013, *AJ*, 146, 32  
 Smith, J. A., Tucker, D. L., Kent, S., et al. 2002, *AJ*, 123, 2121  
 Smolinski, J. P., Lee, Y. S., Beers, T. C., et al. 2011, *AJ*, 141, 89  
 Stetson, P. B. 1987, *PASP*, 99, 191  
 Stoughton, C., Lupton, R. H., Bernardi, M., et al. 2002, *AJ*, 123, 485  
 Tautvaišienė, G., Edvardsson, B., Puzeras, E., & Ilyin, I. 2005, *A&A*, 431, 933  
 Taylor, B. J. 2007, *AJ*, 133, 370  
 Tucker, D. L., Kent, S., Richmond, M. W., et al. 2006, *Astronomische Nachrichten*, 327, 821  
 Yanny, B., Rockosi, C., Newberg, H. J., et al. 2009, *AJ*, 137, 4377  
 York, D. G., Adelman, J., Anderson, J. E., Jr., et al. 2000, *AJ*, 120, 1579  
 Xue, X.-X., Ma, Z., Rix, H.-W., et al. 2014, *ApJ*, 784, 170  
 Xue, X.-X., Rix, H.-W., Ma, Z., et al. 2015, *ApJ*, 809, 144

**Table 1**  
Cluster Properties

ID	Alternate name	$l(^{\circ})^a$	$b(^{\circ})^a$	E(B-V)	$(m - M)_0$	[Fe/H]
M92	NGC 6341	68.34	+34.86	0.02 <sup>e</sup>	14.64 <sup>d</sup>	-2.38 <sup>e</sup>
M13	NGC 6205	59.01	+40.91	0.02 <sup>e</sup>	14.38 <sup>d</sup>	-1.60 <sup>e</sup>
M71	NGC 6838	56.74	-4.56	0.28 <sup>c</sup>	12.86 <sup>c</sup>	-0.81 <sup>e</sup>
Be 29 <sup>k</sup>		197.95	+7.98	0.08	15.6	-0.38
NGC 7789		115.48	-5.37	0.25 <sup>i</sup>	11.33 <sup>j</sup>	-0.04 <sup>k</sup>
NGC 6791		69.96	+10.90	0.16 <sup>b</sup>	13.01 <sup>b</sup>	0.39 <sup>f</sup>

<sup>a</sup> The coordinates are based on the compilation of An et al. (2008) except for NGC 7789 and Berkeley 29.

<sup>b</sup> Brogaard et al. (2011);  $(m - M)_0$  is based on  $(m - M)_V$  assuming  $A_V = 3.1 * E(B - V)$ .

<sup>c</sup> Grundahl et al. (2002);  $(m - M)_0$  derived from Hipparcos (Perryman et al. 1997) subdwarf fitting.

<sup>d</sup> Carretta et al. (2000);  $(m - M)_0$  derived from Hipparcos subdwarf fitting.

<sup>e</sup> Kraft & Ivans (2003); their globular cluster metallicity scale is based on the FeII lines from high-resolution spectra of giants.

<sup>f</sup> We averaged the [Fe/H] measurements of Peterson & Green (1998), Gratton et al. (2006), Carraro et al. (2006) and Brogaard et al. (2011) (+0.40, +0.47, +0.39 and +0.29 respectively).

<sup>g</sup> Anthony-Twarog et al. (2006)

<sup>h</sup> Jacobson et al. (2011)

<sup>i</sup> Bartasiūtė & Tautvaišienė (2004)

<sup>j</sup> Tautvaišienė et al. (2005)

<sup>k</sup> Reddening is from Carraro et al. (2004),  $(m - M)_0$  is from Sestito et al. (2008) and [Fe/H] is the average of the Carraro et al. (2004) and Sestito et al. (2008) values.

<sup>l</sup> Taylor (2007)

<sup>m</sup> An et al. (2007)

<sup>n</sup> Önehag et al. (2014)

**Table 2**  
Plate Information for Clusters in this Paper

Cluster ID	Alternate	Plate	MJD	Plate type
M92	NGC 6341	2247	53857	Offset
M92	NGC 6341	2247	54169	Bright
M92	NGC 6341	2256	53859	Faint
M13	NGC 6205	2255	53565	Offset
M13	NGC 6205	2255	53565	Very Bright
M13	NGC 6205	2174	53521	Bright
M13	NGC 6205	2185	53532	Faint
M71	NGC 6838	2333	53682	
M71	NGC 6838	2338	53679	
Be 29		3334	54927	
Be 29		3335	54922	
NGC 7789		2337	53991	Bright
NGC 6791		2800	54326	Bright
NGC 6791		2821	54393	Faint

**Table 3**  
M92 Members Observed by SEGUE

Plate	MJD	Fiber	$r$ (mag.)	error (mag.)	$g-r$ (mag.)	$g-i$ (mag.)	$g-z$ (mag.)	RA (2000)	Dec (2000)	Velocity (km s <sup>-1</sup> )	Phot. ref.	PM prob (%)
2247	53857	402	14.456	0.006	0.621	0.893	1.040	259.1997	43.1044	-114.6	1	99
2247	53857	403	14.218	0.006	0.607	0.884	1.047	259.1831	43.1255	-103.4	1	99
2247	53857	412	13.410	0.002	0.656	0.963	1.148	259.1429	43.1268	-113.3	1	99
2247	53857	416	13.448	0.003	0.642	0.948	1.128	259.1572	43.1448	-122.2	1	99
2247	53857	444	13.592	0.003	0.636	0.943	1.116	259.2514	43.1966	-109.5	1	99
2247	53857	449	13.226	0.002	0.723	1.065	1.234	259.2452	43.2532	-107.9	1	99
2247	53857	453	14.333	0.038	0.583	0.842	0.976	259.2280	43.1740	-110.0	1	99
2247	53857	455	12.462	0.004	0.857	1.252	1.454	259.2078	43.1781	-115.4	1	99
2247	53857	458	13.109	0.002	0.752	1.107	1.276	259.2406	43.2365	-118.0	1	99
2247	53857	460	13.813	0.011	0.634	0.969	1.142	259.2313	43.0843	-120.1	1	99
2247	53857	486	14.586	0.005	0.596	0.865	1.027	259.1491	42.9443	-118.5	1	...
2247	53857	514	14.344	0.003	0.596	0.877	1.028	259.2487	43.0183	-119.8	1	99
2247	53857	516	14.285	0.005	0.420	0.614	0.684	259.2202	43.0582	-110.1	1	99
2247	53857	522	11.619	0.006	1.159	1.659	1.930	259.3405	43.2149	-103.4	1	99
2247	53857	523	12.740	0.003	0.809	1.176	1.360	259.3189	43.1792	-104.6	1	99
2247	53857	525	14.024	0.014	0.658	0.933	1.095	259.3403	43.1842	-110.7	1	99
2247	53857	526	11.961	0.011	0.970	1.441	1.702	259.2935	43.1855	-106.2	1	99
2247	53857	529	13.895	0.005	0.556	0.824	0.980	259.3320	43.2451	-112.3	1	99
2247	53857	532	14.305	0.009	0.476	0.691	0.818	259.3376	43.1035	-108.7	1	99
2247	53857	537	14.332	0.006	0.609	0.887	1.032	259.3146	43.0831	-113.3	1	99
2247	53857	553	14.833	0.001	0.341	0.486	0.583	259.3048	43.0001	-102.9	1	99
2247	53857	559	14.371	0.005	0.595	0.875	1.033	259.2664	43.0341	-110.2	1	99
2247	53857	572	12.407	0.003	0.856	1.230	1.459	259.3821	43.0949	-107.3	1	99
2247	53857	576	14.507	0.010	0.599	0.879	1.035	259.3699	43.1675	-114.0	1	99
2247	53857	577	14.691	0.004	0.571	0.831	0.982	259.3709	43.1153	-114.1	1	99
2247	53857	580	14.353	0.009	0.598	0.883	1.020	259.3730	43.2041	-113.7	1	99
2247	53857	583	13.489	0.005	0.690	1.004	1.200	259.3425	43.0805	-112.8	1	99
2247	53857	609	14.660	0.005	0.606	0.871	0.998	259.5197	43.1712	-118.5	2	84
2247	53857	612	14.889	0.002	0.566	0.832	0.977	259.4598	43.2295	-105.3	1	...
2247	54169	361	15.583	0.004	-0.225	-0.395	-0.463	259.0527	43.1739	-115.1	1	...
2247	54169	380	15.664	0.002	0.522	0.749	0.904	259.1245	43.1009	-109.5	1	...
2247	54169	408	14.865	0.007	0.567	0.816	0.973	259.1516	43.1156	-120.0	1	99
2247	54169	418	15.063	0.003	0.570	0.810	0.959	259.1925	43.0829	-119.6	1	99
2247	54169	441	15.760	0.002	-0.316	-0.533	-0.641	259.2120	43.1897	-115.4	1	...
2247	54169	444	15.590	0.003	0.499	0.740	0.871	259.1783	43.2465	-112.3	1	...
2247	54169	449	15.015	0.003	0.549	0.800	0.946	259.2012	43.1713	-116.5	1	...
2247	54169	451	15.753	0.003	0.527	0.744	0.888	259.2681	43.0696	-121.9	1	...
2247	54169	452	15.565	0.005	0.495	0.746	0.897	259.1898	43.2296	-121.4	1	...
2247	54169	484	14.586	0.005	0.596	0.865	1.027	259.1490	42.9443	-115.0	1	...
2247	54169	504	14.638	0.022	0.554	0.839	1.002	259.3471	42.9488	-112.1	1	...
2247	54169	521	15.651	0.004	-0.273	-0.454	-0.545	259.2528	43.2175	-119.3	1	99
2247	54169	526	15.592	0.004	-0.257	-0.447	-0.527	259.2901	43.0796	-117.6	1	99







Table 4 — *Continued*

Plate	MJD	Fiber	$r$ (mag.)	error (mag.)	$g-r$ (mag.)	$g-i$ (mag.)	$g-z$ (mag.)	RA (2000)	Dec (2000)	Velocity (km s <sup>-1</sup> )	Phot. ref.	PM prob (%)
2255	53565	175	15.232	0.002	0.577	0.824	0.919	250.3261	36.3471	-242.6	1	99
2255	53565	178	13.710	0.002	0.721	1.019	1.206	250.4017	36.2855	-242.2	1	99
2255	53565	426	15.024	0.001	0.571	0.831	0.989	250.3146	36.5174	-244.4	1	99
2255	53565	428	14.245	0.007	0.672	0.957	1.123	250.2309	36.5953	-250.2	1	99
2255	53565	431	13.412	0.021	0.728	1.065	1.255	250.3326	36.4106	-250.0	1	99
2255	53565	433	15.370	0.005	-0.263	-0.450	-0.555	250.2911	36.5694	-241.9	1	99
2255	53565	436	14.753	0.003	0.619	0.885	1.026	250.3078	36.4174	-241.8	1	99
2255	53565	440	14.721	0.003	0.616	0.874	1.023	250.2608	36.4377	-247.5	1	99
2255	53565	464	13.338	0.003	0.703	1.005	1.178	250.3784	36.5035	-244.4	1	99
2255	53565	465	15.230	0.004	-0.209	-0.366	-0.484	250.4422	36.4292	-245.7	1	99
2255	53565	468	15.375	0.008	0.538	0.810	0.891	250.3910	36.4529	-242.3	1	98
2255	53565	472	14.576	0.002	0.621	0.888	1.037	250.3964	36.4008	-241.8	1	99
2255	53565	474	13.116	0.003	0.797	1.132	1.301	250.3681	36.4510	-243.0	1	98
2255	53565	475	13.420	0.002	0.753	1.087	1.280	250.3134	36.4899	-244.4	1	99
2255	53565	477	13.740	0.002	0.697	0.997	1.154	250.3787	36.4254	-249.1	1	99
2255	53565	482	15.116	0.002	-0.187	-0.328	-0.421	250.3339	36.6145	-250.0	1	99
2255	53565	486	14.665	0.001	0.611	0.886	1.050	250.3160	36.5549	-243.1	1	99
2255	53565	487	12.527	0.009	0.917	1.283	1.512	250.4381	36.4702	-239.1	1	99
2255	53565	490	15.825	0.003	0.517	0.755	0.889	250.3626	36.5661	-244.7	1	...
2255	53565	491	11.564	0.002	1.277	1.791	2.111	250.4595	36.4042	-247.7	1	99
2255	53565	493	13.683	0.013	0.722	1.035	1.204	250.4420	36.4546	-248.3	1	99
2255	53565	496	14.258	0.007	0.649	0.941	1.100	250.3886	36.5412	-248.9	1	99
2255	53565	498	11.446	0.014	1.352	1.938	2.281	250.4247	36.4476	-247.8	1	99
2255	53565	499	13.324	0.001	0.771	1.090	1.290	250.4365	36.3909	-243.3	1	99
2255	53565	501	13.201	0.004	0.783	1.128	1.314	250.4386	36.5185	-243.5	1	99
2255	53565	503	13.964	0.002	0.687	0.993	1.145	250.4857	36.5007	-246.4	1	99
2255	53565	504	13.826	0.004	0.705	1.019	1.167	250.4200	36.5698	-248.5	1	99
2255	53565	505	15.367	0.003	-0.231	-0.388	-0.488	250.4430	36.5538	-246.8	1	99
2255	53565	510	15.115	0.001	0.595	0.867	0.999	250.4508	36.5948	-248.2	1	99
2255	53565	516	11.578	0.011	1.332	1.893	2.207	250.4620	36.4817	-242.5	1	99
2255	53565	517	13.955	0.010	0.687	1.002	1.124	250.4654	36.4590	-241.8	1	99
2255	53565	519	14.040	0.002	0.680	0.970	1.129	250.5015	36.4235	-243.7	1	99
2255	53565	520	14.373	0.004	0.644	0.930	1.042	250.4717	36.4231	-241.2	1	99
2255	53565	542	14.977	0.003	0.589	0.843	0.980	250.5715	36.5259	-246.9	1	99
2255	53565	544	14.561	0.004	0.637	0.912	1.067	250.5411	36.4955	-249.4	1	99
2255	53565	547	14.579	0.003	0.633	0.910	1.043	250.5786	36.5043	-249.4	1	99
2255	53565	548	14.836	0.002	0.629	0.887	1.037	250.5392	36.5664	-245.2	1	99
2255	53565	549	14.523	0.005	0.637	0.908	1.051	250.5105	36.5424	-249.2	1	99
2255	53565	550	15.197	0.004	0.589	0.842	0.956	250.5207	36.5268	-246.5	1	99
2255	53565	551	14.674	0.004	0.620	0.886	1.020	250.6084	36.4513	-243.3	1	99
2255	53565	552	13.934	0.002	0.689	0.988	1.149	250.5688	36.4162	-241.4	1	99
2255	53565	553	14.842	0.004	0.606	0.864	1.013	250.5565	36.4768	-239.5	1	99
2255	53565	557	14.463	0.002	0.635	0.906	1.054	250.5687	36.4371	-239.6	1	99
2255	53565	589	14.717	0.003	0.617	0.876	1.033	250.5795	36.6176	-245.9	1	99
2255	53565	600	14.507	0.001	0.651	0.910	1.078	250.5424	36.6308	-248.7	1	98
2255	53565	500	14.532	0.005	0.621	0.913	1.029	250.3637	36.5395	-240.6	2	99

References. — 1. Clem et al. (2008), 2. An et al. (2008)

Table 5  
M71 members observed by SEGUE

Plate	MJD	Fiber	$r$ (mag.)	error (mag.)	$g-r$ (mag.)	error (mag.)	E(B-V) offset	RA (2000)	Dec (2000)	Velocity (km s <sup>-1</sup> )	error (km s <sup>-1</sup> )	PM prob (%)	ID
2333	53682	163	11.766	...	1.480	...	-0.01	298.4511	18.8007	-20.5	0.2	97	1-45
2333	53682	167	14.106	0.002	0.828	0.004	0.00	298.4630	18.7697	-26.2	0.6	85	1-19
2333	53682	173	12.477	0.002	1.273	0.004	0.00	298.4610	18.8189	-24.9	0.3	97	1-53
2333	53682	185	12.886	...	1.051	...	-0.02	298.4210	18.7683	-23.2	0.5	96	1-95
2333	53682	191	14.203	0.004	1.069	0.005	0.04	298.4241	18.8108	-25.3	0.8	95	1-59
2333	53682	224	13.695	0.004	1.114	0.008	0.03	298.3947	18.7727	-23.4	0.4	95	KC-39
2333	53682	225	12.407	0.003	1.347	0.004	0.05	298.4062	18.7500	-26.2	0.3	94	A9
2333	53682	239	12.072	...	1.488	...	0.02	298.4066	18.7914	-26.7	0.3	90	1-77
2338	53679	150	12.729	0.004	1.104	0.004	0.00	298.4511	18.8071	-21.6	0.5	97	1-56

**Table 6**  
Variable Reddening Values (in  $E(B-V)$ ) for M71

Dec offset (arcsec)	RA offset (arcsec)									
	-225	-175	-125	-75	-25	25	75	125	175	225
-225	0.03	0.02	0.00	-0.01	-0.01	0.00	0.00	0.00	0.00	0.03
-175	0.04	0.03	0.03	0.01	-0.01	-0.01	0.00	0.00	0.00	0.02
-125	0.02	0.03	0.08	0.02	-0.02	-0.02	-0.01	0.00	0.01	0.03
-75	0.03	0.02	0.02	-0.02	-0.02	-0.02	-0.02	0.00	0.02	0.02
-25	0.03	0.03	0.03	-0.02	0.00	0.00	0.00	0.00	0.02	0.01
25	0.04	0.04	0.02	0.01	0.01	0.00	0.00	0.01	0.00	0.00
75	0.04	0.04	0.03	0.02	0.02	-0.01	-0.01	0.0	0.0	-0.01
125	0.05	0.05	0.05	0.04	-0.01	0.00	0.00	0.00	0.00	-0.01
175	0.06	0.05	0.04	0.02	0.00	0.00	0.00	0.00	0.00	0.00
225	0.07	0.06	0.05	0.05	0.02	0.00	0.00	-0.01	-0.01	-0.01

**Table 7**  
NGC 7789 Members Observed by SEGUE

Plate	MJD	Fiber	$V$ (mag.)	$V - I$ (mag.)	$(g - r)_0$ (transf)	RA (2000)	Dec (2000)	$E(B - V)$	Velocity ( $\text{km s}^{-1}$ )
2377	53991	151	12.794	1.336	0.820	359.5293	56.6800	0.25	-49.1
2377	53991	162	12.839	1.284	0.765	359.3542	56.6434	0.25	-46.7
2377	53991	175	12.913	1.288	0.730	359.3507	56.6600	0.27	-50.6
2377	53991	176	13.055	1.306	0.800	359.3866	56.6721	0.25	-48.0
2377	53991	178	12.962	1.331	0.795	359.3378	56.5841	0.24	-47.6
2377	53991	191	12.981	1.310	0.763	359.2386	56.6153	0.25	-44.4
2377	53991	200	12.273	1.539	1.012	359.2176	56.5608	0.25	-44.6
2377	53991	232	12.188	1.528	1.048	358.9569	56.6550	0.25	-48.1
2377	53991	439	13.260	1.316	0.794	359.1707	56.6964	0.25	-46.8
2377	53991	461	12.305	1.540	1.016	359.2311	56.7525	0.27	-46.2
2377	53991	489	12.982	1.344	0.824	359.2382	56.6971	0.25	-50.7
2377	53991	493	13.111	1.328	0.823	359.2648	56.7225	0.25	-47.5
2377	53991	494	13.160	1.349	0.829	359.1855	56.7149	0.25	-47.6
2377	53991	506	11.986	1.617	1.109	359.5007	56.8368	0.26	-47.1
2377	53991	515	13.164	1.377	0.844	359.4409	56.8448	0.25	-47.6

**Table 8**  
NGC 6791 Members Observed by SEGUE

Plate	MJD	Fiber	$r$ (mag.)	error (mag.)	$g - r$ (mag.)	$g - i$ (mag.)	$g - z$ (mag.)	RA (2000)	Dec (2000)	Velocity ( $\text{km s}^{-1}$ )	PM prob (%)
2800	54326	151	16.943	0.005	0.927	1.235	1.439	290.3105	37.7758	-47.6	88
2800	54326	152	17.904	0.011	0.687	0.915	1.070	290.2779	37.8023	-45.8	96
2800	54326	154	15.327	0.006	1.100	1.495	1.745	290.2560	37.8014	-47.1	90
2800	54326	156	16.112	0.005	1.040	1.395	1.639	290.2894	37.7840	-43.9	75
2800	54326	159	14.061	0.005	1.118	1.528	1.762	290.2762	37.7499	-45.8	99
2800	54326	160	15.923	0.004	1.018	1.369	1.577	290.3084	37.7526	-47.2	85
2800	54326	161	17.126	0.007	0.893	1.195	1.361	290.2689	37.7212	-46.5	97
2800	54326	167	13.923	0.007	1.329	...	2.178	290.2547	37.7037	-47.7	68
2800	54326	169	14.148	0.007	1.160	1.583	1.820	290.2448	37.7203	-45.3	77
2800	54326	170	13.545	0.006	1.440	...	2.484	290.2191	37.7412	-47.9	92
2800	54326	172	17.284	0.006	0.736	0.955	1.086	290.2085	37.7977	-45.3	79
2800	54326	173	17.085	0.007	0.972	1.314	1.497	290.2308	37.7971	-47.9	81
2800	54326	174	14.073	0.005	1.195	1.625	1.895	290.2536	37.7594	-46.8	97
2800	54326	175	14.109	0.005	1.166	1.572	1.836	290.2536	37.7777	-49.5	97
2800	54326	180	14.095	0.004	1.126	1.520	1.767	290.2203	37.7592	-45.5	93
2800	54326	181	14.421	0.003	1.204	1.656	1.926	290.1882	37.7428	-49.6	98
2800	54326	182	17.435	0.007	0.668	0.893	0.968	290.1303	37.7752	-47.3	98
2800	54326	183	14.143	0.006	1.145	1.541	1.812	290.1889	37.7883	-52.4	88
2800	54326	184	17.368	0.009	0.657	0.878	0.979	290.1277	37.7548	-50.6	98
2800	54326	185	14.387	0.005	1.142	1.527	1.775	290.1635	37.7437	-46.8	98
2800	54326	187	17.154	0.007	0.751	0.998	1.146	290.1433	37.8011	-47.0	73
2800	54326	188	17.932	0.007	0.704	0.933	1.052	290.1961	37.7612	-45.8	91
2800	54326	189	16.560	0.009	0.992	1.324	1.518	290.1688	37.7852	-45.9	55

Table 8 — *Continued*

Plate	MJD	Fiber	$r$ (mag.)	error (mag.)	$g-r$ (mag.)	$g-i$ (mag.)	$g-z$ (mag.)	RA (2000)	Dec (2000)	Velocity (km s <sup>-1</sup> )	PM prob (%)
2800	54326	190	15.701	0.006	1.064	1.439	1.672	290.1767	37.7642	-46.3	88
2800	54326	194	17.300	0.011	0.642	0.852	0.968	290.1742	37.7060	-52.4	77
2800	54326	197	15.979	0.007	1.025	1.377	1.606	290.1808	37.7214	-46.7	92
2800	54326	199	14.094	0.004	1.287	...	2.107	290.1639	37.8013	-45.7	94
2800	54326	431	17.103	0.005	0.736	0.993	1.109	290.1247	37.8115	-40.9	98
2800	54326	465	14.972	0.004	1.139	1.570	1.844	290.2405	37.8170	-44.9	85
2800	54326	475	14.774	0.010	1.128	1.540	1.823	290.1927	37.8196	-43.2	99
2800	54326	479	17.874	0.008	0.691	0.947	1.064	290.1633	37.8346	-46.8	95
2800	54326	480	17.249	0.007	0.759	1.039	1.180	290.1579	37.8190	-44.4	82
2821	54393	141	17.951	0.008	0.721	0.946	1.066	290.2928	37.7322	-46.8	89
2821	54393	142	18.703	0.010	0.839	1.086	1.255	290.2954	37.7891	-40.9	96
2821	54393	145	17.970	0.008	0.672	0.911	0.956	290.3149	37.7871	-44.0	68
2821	54393	146	18.216	0.009	0.707	0.936	1.065	290.2860	37.7175	-43.9	68
2821	54393	149	17.586	0.006	0.674	0.878	0.966	290.2926	37.7521	-43.2	70
2821	54393	161	17.537	0.008	0.661	0.865	0.976	290.2675	37.7325	-48.9	83
2821	54393	165	18.742	0.012	0.822	1.119	1.234	290.1696	37.7074	-48.6	67
2821	54393	166	18.509	0.010	0.776	1.027	1.210	290.2165	37.7927	-43.8	85
2821	54393	167	18.392	0.013	0.772	1.037	1.095	290.2531	37.7614	-43.8	91
2821	54393	169	18.398	0.013	0.777	1.042	1.203	290.2357	37.7495	-43.6	94
2821	54393	172	18.174	0.011	0.754	0.991	1.120	290.2331	37.7795	-48.4	69
2821	54393	173	18.094	0.013	0.715	0.941	1.043	290.2340	37.7255	-46.5	76
2821	54393	174	18.263	0.014	0.736	0.934	1.075	290.2744	37.7682	-46.9	80
2821	54393	176	18.983	0.014	0.850	1.154	1.265	290.2389	37.7979	-42.3	63
2821	54393	177	18.312	0.011	0.757	1.000	1.151	290.2552	37.7811	-44.8	92
2821	54393	178	18.462	0.011	0.787	1.051	1.215	290.2708	37.7936	-47.7	84
2821	54393	179	17.434	0.013	0.698	0.925	1.037	290.2332	37.6950	-46.3	61
2821	54393	182	18.009	0.008	0.738	0.964	1.044	290.1917	37.7502	-44.9	98
2821	54393	183	17.738	0.009	0.668	0.870	0.983	290.1618	37.7224	-48.2	68
2821	54393	187	17.646	0.009	0.646	0.868	0.972	290.1851	37.7333	-49.2	72
2821	54393	188	18.770	0.010	0.878	1.157	1.295	290.1615	37.7461	-42.9	72
2821	54393	190	19.206	0.018	0.969	1.265	1.434	290.2118	37.7134	-43.0	85
2821	54393	191	18.251	0.011	0.732	0.980	1.100	290.1620	37.7770	-50.4	95
2821	54393	193	18.495	0.009	0.814	1.069	1.168	290.1486	37.7595	-44.2	97
2821	54393	194	18.047	0.009	0.737	0.971	1.087	290.1838	37.7774	-45.6	95
2821	54393	195	18.852	0.012	0.842	1.122	1.293	290.2029	37.7670	-44.5	89
2821	54393	196	18.058	0.012	0.708	0.939	1.101	290.2135	37.7412	-48.2	97
2821	54393	197	17.757	0.006	0.664	0.888	0.988	290.1443	37.7864	-47.3	94
2821	54393	198	18.678	0.012	0.819	1.105	1.209	290.1754	37.7626	-48.5	68
2821	54393	199	18.890	0.014	0.867	1.150	1.331	290.1903	37.7149	-48.0	72
2821	54393	200	18.260	0.011	0.751	0.974	1.090	290.1816	37.7957	-47.5	56
2821	54393	232	19.101	0.016	0.954	1.342	1.515	290.1246	37.7310	-46.9	87
2821	54393	235	17.550	0.009	0.689	0.900	0.991	290.1257	37.7643	-42.1	95
2821	54393	436	18.307	0.008	0.774	1.082	1.253	290.1259	37.8133	-44.3	91
2821	54393	439	17.568	0.006	0.688	0.926	1.027	290.1193	37.7980	-44.1	98

Table 9  
Berkeley 29 members observed by SEGUE

Plate	MJD	Fiber	$g$ (mag.)	error (mag.)	$g-r$ (mag.)	error (mag.)	RA (2000)	Dec (2000)	Velocity (km s <sup>-1</sup> )	error (km s <sup>-1</sup> )	other ID <sup>a</sup>
3335	54922	113	19.110	0.015	0.599	103.3311	16.8730	0.017	26.57	2.22	
3335	54922	195	16.799	0.007	0.761	103.1608	16.8460	0.011	34.56	1.04	
3335	54922	462	18.926	0.011	0.658	103.2417	16.9463	0.018	39.85	1.85	
3335	54922	474	19.288	0.014	0.597	103.1888	16.8793	0.021	18.02	2.80	
3335	54922	481	17.039	0.006	0.746	103.2836	16.9279	0.008	17.01	0.86	S398,C801,F948
3335	54922	495	17.118	0.007	0.779	103.3010	16.9836	0.010	17.81	0.95	F1437
3335	54922	496	17.074	0.006	0.776	103.2311	16.9610	0.009	18.13	0.89	S602
3335	54922	497	17.120	0.008	0.778	103.2566	16.9392	0.010	18.22	0.85	S159
3335	54922	498	18.165	0.007	0.701	103.2626	16.9245	0.011	21.69	1.34	
3335	54922	508	18.076	0.011	0.718	103.2837	16.9631	0.015	16.68	1.53	

<sup>a</sup> Identifications are from S: Sestito et al. (2008), C: Carraro et al. (2004) and F: Frinchaboy et al. (2006).